Modelling lateral meltwater flow and superimposed ice formation atop Greenland's near-surface ice slabs

Journal:	*Journal of Glaciology*
Manuscript ID	JOG-23-0116.R1
Manuscript Type:	Article
Date Submitted by the Author:	n/a
Complete List of Authors:	Clerx, Nicole; University of Fribourg, Geoscience Machguth, Horst; University of Fribourg Department of Geosciences, Department of Geosciences Tedstone, Andrew; University of Fribourg, Department of Geosciences Van As, Dirk; GEUS, Glaciology and Climate
Keywords:	Glacier hydrology, Glaciological model experiments, Melt - surface, Snow/ice surface processes, Ice-sheet mass balance
Abstract:	At high elevations on the Greenland ice sheet meltwater percolates and refreezes in place, and hence does not contribute to mass loss. However, meltwater generation and associated surface runoff is occurring from increasingly higher altitudes, causing changes in firn stratigraphy that have led to the presence of near-surface ice slabs. These ice slabs force meltwater to flow laterally instead of percolating downwards. Here we present a simple, physics-based quasi 2D-model to simulate lateral meltwater runoff and superimposed ice formation on top of ice slabs. Using an Eulerian Darcy flow scheme, the model calculates how far meltwater can travel within a melt season and when it appears at the snow surface. Results show that lateral flow is a highly efficient mechanism for runoff, as in any model grid cell lateral outflow is over 30 times larger than the amount of meltwater generated in situ. Superimposed ice formation can retain up to 40% of the available meltwater, and generally delays visible runoff. Validating the model against field or remote sensing data remains challenging, but the results

	presented here are a first step towards a more comprehensive understanding and description of the hydrological system in the accumulation zone of the southwestern Greenland ice sheet.

Modelling lateral meltwater flow and superimposed ice formation atop Greenland's near-surface ice slabs

Nicole Clerx,[1] Horst Machguth,[1] Andrew J. Tedstone,[1] Dirk van As[2]

[1]*Department of Geoscience, University of Fribourg, Fribourg, Switzerland*

[2]*Geological Survey of Denmark and Greenland (GEUS), Copenhagen, Denmark*

Correspondence: Nicole Clerx <nicole.clerx@unifr.ch>

ABSTRACT. At high elevations on the Greenland ice sheet meltwater percolates and refreezes in place, and hence does not contribute to mass loss. However, meltwater generation and associated surface runoff is occurring from increasingly higher altitudes, causing changes in firn stratigraphy that have led to the presence of near-surface ice slabs. These ice slabs force meltwater to flow laterally instead of percolating downwards. Here we present a simple, physics-based quasi 2D-model to simulate lateral meltwater runoff and superimposed ice formation on top of ice slabs. Using an Eulerian Darcy flow scheme, the model calculates how far meltwater can travel within a melt season and when it appears at the snow surface. Results show that lateral flow is a highly efficient mechanism for runoff, as in any model grid cell lateral outflow is over 30 times larger than the amount of meltwater generated in situ. Superimposed ice formation can retain up to 40% of the available meltwater, and generally delays visible runoff. Validating the model against field or remote sensing data remains challenging, but the results presented here are a first step towards a more comprehensive understanding and description of the hydrological system in the accumulation zone of the southwestern Greenland ice sheet.

INTRODUCTION

The Greenland ice sheet is losing mass at an accelerating rate, and since around the year 2000 the surface mass balance has become the dominant driver of ice sheet mass loss (van den Broeke and others, 2016; Bamber and others, 2018; the IMBIE Team, 2019). Increasing summer meltwater generation and associated runoff is the main driver of the declining surface mass balance, in particular in the southwestern part of the Greenland ice sheet (Nienow and others, 2017; van den Broeke and others, 2017; Mouginot and others, 2019). From 1996 onwards, there has been a clear acceleration in meltwater runoff and discharge (Enderlin and others, 2014; van den Broeke and others, 2016).

This increase in runoff coincides with an expansion of the area in which mass loss occurs: as a result of higher summer temperatures and record melt events, surface melt and runoff have increasingly occurred from higher elevations in recent years (Hanna and others, 2008; Nghiem and others, 2012; van As and others, 2012; McGrath and others, 2013; Ahlstrøm and others, 2017). In this context, we distinguish between the runoff limit and the visible runoff limit. The runoff limit is the highest elevation from which at least part of the locally generated meltwater flows towards the ice sheet margin and contributes to mass loss, i.e. where meltwater input exceeds the retention capacity of snow and firn (e.g. Pfeffer and others, 1991; Reeh, 1991; Braithwaite and others, 1994). Refreezing can occur below the runoff limit, but is not sufficient to retain all the meltwater generated in situ. Above the runoff limit all meltwater refreezes locally and does not contribute to mass loss; the runoff limit location and its migration throughout the melt season therefore plays an important role in the ice sheet surface mass balance (van As and others, 2016; Nienow and others, 2017). We define the visible runoff limit as the uppermost altitude at which liquid meltwater is visible at the surface and drains through surface streams and river networks, similar to Müller (1962).

Since 2010, a series of extraordinarily warm summers has occurred. In 2010, 2012 and 2019 surface melt covered nearly all of the ice sheet (Nghiem and others, 2012; Tedesco and Fettweis, 2020). Melting at high elevation causes structural changes in snow and firn, partly by enhanced densification rates upon the first introduction of liquid water and snow grain metamorphosis (Brun, 1989; Marshall and others, 1999), but also by refreezing of meltwater forming infiltration ice bodies such as ice glands, lenses and layers within the snow and firn (Benson, 1962).

Ice sheet-wide, between 1985 and 2020, the maximum visible runoff limit rose by on average 194 metres, expanding the visible runoff area by around 29% (Tedstone and Machguth, 2022). This observed

rise in the visible runoff limit may be attributed to changes in firn stratigraphy caused by the intensive meltwater refreezing following extreme melt summers. These events have led to the formation of thick ice layers, also called ice slabs, which have been identified in firn cores and through airborne radar data since 2010 (Machguth and others, 2016; MacFerrin and others, 2019). These ice slabs act as aquitards, forcing meltwater to runoff laterally rather than allowing it to percolate to depth. Recent studies furthermore show that significant melt events directly impact the occurrence, distribution and thickness of near-surface ice slabs (Culberg and others, 2021; Jullien and others, 2023).

Under melting conditions, slush fields develop on top of near-surface ice slabs at different elevations in the accumulation zone of the southwestern Greenland ice sheet. Slush fields are water-saturated areas of snow and firn with visible meltwater ponding on the surface, and constitute an important component in the hydrological system strongly linked to runoff (Holmes, 1955). Field observations show that meltwater flows laterally through the slush matrix before fully saturating the snowpack and causing slush fields to become visible on the ice sheet surface (Clerx and others, 2022). The prerequisites for the transition from vertical water percolation to lateral meltwater flow, as well as the exact processes driving the evolution of slush fields from their first appearance to subsequent drainage, however, remain unclear.

A common approach for modelling meltwater flow through snow and firn is the bucket scheme. Here, the firn is vertically divided into layers, and after exceeding a set threshold value for water saturation, water moves between model layers instantaneously. Once reaching the bottommost grid cell in the vertical domain or another impermeable grid cell, immediate runoff takes place hence mimicking lateral meltwater flow. Bucket schemes are applied in the main regional climate models (RCMs) used for predicting the Greenland ice sheet mass balance, the Regional Atmospheric Climate Model (RACMO; Noël and others, 2019), the Modèle Atmosphérique Régional (MAR; Fettweis and others, 2017) and HIRHAM (Bøssing Christensen and others, 2007). In RACMO, the bucket scheme is enhanced by its coupling to a simplified version of the IMAU-FDM (Firn Densification Model) to simulate changes in firn properties and meltwater percolation (Ligtenberg and others, 2011; Kuipers Munneke and others, 2014, 2015; Noël and others, 2018). The HIRHAM model also uses an enhanced bucket scheme to approximate lateral meltwater runoff (Langen and others, 2017), as water in excess of the irreducible water saturation runs off only after a certain characteristic residence time τ_{RO} that is related to local slope (Zuo and Oerlemans, 1996). Another approach for water flow through snow employs the Richards equation, and is used in models like SNOWPACK (Bartelt and Lehning, 2002; Lehning and others, 2002) or for example the continuum model by Meyer and Hewitt (2017).

The disadvantage of these more complicated models is their computation time, which makes integration with already CPU-heavy RCMs challenging. All of the models mentioned here operate along a vertical axis only, and hence do not explicitly model lateral meltwater flow.

For capturing lateral liquid water transport in a snowpack on a multi-km scale the bucket scheme is robust and useful, as simplified models have been shown to provide runoff predictions that closely match those of significantly more complex snow-physics models (Magnusson and others, 2015). However, existing parametrisations for meltwater processes, and estimates of refreezing and retention in the surface mass balance simulated by RCMs, remain major contributors to the total uncertainty in future mass balance predictions (Smith and others, 2017; Nienow and others, 2017). This uncertainty is highlighted when comparing the surface runoff area modelled by two RCMs to satellite-based observations: the RCMs overestimate the surface runoff area by 16-30% (Tedstone and Machguth, 2022). Vandecrux and others (2020) evaluated nine different firn models in the Retention Model Intercomparison Project RetMIP, and found that the model spread in meltwater retention and runoff quantities increases with increasing meltwater input. Refreezing could account for retention of up to almost half (40-46%) of the total amount of liquid water input on the Greenland ice sheet, although this estimate remains highly ambiguous given the lack of understanding of the importance of specific hydrological processes in firn (Steger and others, 2017). These findings emphasize the significant uncertainty regarding the fate of meltwater, especially when considering future ice sheet mass balance scenarios in a warming climate.

Improving estimates of total runoff from RCMs requires more knowledge of the hydrological processes at and around the runoff limit. Furthermore, this increased understanding of meltwater hydrology should be more effectively integrated into RCMs. In mountain hydrology, numerous sophisticated (2D) models exist that route water through different reservoirs in a hydrological catchment and couple surface- and subsurface flow, like for example the mesoscale Hydrological Model (mHM; Samaniego and others, 2010; Kumar and others, 2013), the ParFlow-Community Land Model (Maxwell and Miller, 2005; Kollet and Maxwell, 2006) and MODFLOW (McDonald and Harbaugh, 1988; Harbaugh and others, 2000). However, initialisation and calibration of these models generally requires a lot of (small-scale) field observations, and the complex calculations in these models often prohibit a thorough interpretation of results. A conceptual 2D-model for perennial firn aquifers using the modified ground water model SUTRA-ICE was recently published (Miller and others, 2022), but this model is not suitable in scenarios where near-surface ice slabs play an important role in the hydrological system. This limitation arises primarily from its use of a fixed,

constant snow depth, which fails to accurately represent cases where surface lowering due to melt plays an important role, such as when the snowpack on top of the ice slab is relatively thin.

In this paper we present a quasi 2D-model of runoff, that simulates lateral meltwater flow and refreezing on top of an ice slab on the southwest Greenland ice sheet. In our simple, low-CPU-intensive model we use an Eulerian Darcy flow scheme to calculate (i) the distance meltwater can travel before fully saturating the snowpack and hence becoming visible at the snow surface within a melt season, and (ii) when this meltwater breakthrough at the surface (i.e. slush formation) occurs. The ultimate goal of the model is to reproduce the evolution of water table height throughout the melt season, to investigate the total amount of meltwater present between the visible and actual runoff limits. This would help to quantify the amount of water available for refreezing, which contributes to the further thickening of near-surface ice slabs, and the amount of meltwater runoff.

STUDY AREA AND CLIMATOLOGICAL SETTING

Our study region is the southwest of the Greenland ice sheet around 67◦N, 47◦W near the upper end of the K-transect, a 140-km transect of stakes and automatic weather stations monitoring ice sheet surface mass balance at various elevations since 1990 (van de Wal and others, 2005, 2012; Fausto and others, 2021). Ice slabs have been identified at elevations up to 1900 m a.s.l. here (Machguth and others, 2016; Jullien and others, 2023), and the maximum annual visible runoff limit since 2012 ranges from 1650-∼1840 m a.s.l. (Tedstone and Machguth, 2022; Machguth and others, 2022). Extensive meteorological data is available from the nearby PROMICE weather stations, of which KAN_M and KAN_U, at respectively 1270 and 1840 m a.s.l., are the two weather stations used for this study (Ahlstrøm and others, 2008; How and others, 2022).

Since 2010, average winter accumulation in the study area was approximately 0.3–0.4 m w.e. (e.g. Ahlstrøm and others, 2017; Smeets and others, 2018; How and others, 2022), and the equilibrium line altitude (ELA) is gradually migrating upwards. In the period from 1990–2011 the average ELA was at 1553 m a.s.l. (van de Wal and others, 2012). The mean annual air temperature for the years 2008 to 2020 at KAN_U was -14.8 ◦C (Fausto and others, 2021), and in the period from 2011 to 2021 the melt season counted between 12 and 47 positive degree days in the area of interest (Xiao and others, 2022). Average surface slope between 1900 and 1700 m a.s.l. in the study area is -0.005 m m^{-1}, equivalent to an elevation loss of approximately 5 m over 1 km according to the ArcticDEM (Porter and others, 2018).

METHODS

In this section, we first introduce the model concept and describe the parameters governing the timing and location of visible runoff appearance, including the various modelled melt scenarios. Next, we provide a more comprehensive description of the most important modelled processes individually. Finally, we describe how we assessed the model sensitivity to the most influential input parameters.

Our model is based on Darcy's law for flow through a porous medium. It consists of a downslope transect of grid cells (Fig. 1) in which each grid cell has a fixed initial height, consists of isothermal dry snow at 0∘C at the start of every model run ($t = 0$), and is underlain by solid ice. Each grid cell is divided into two domains: (i) vertical percolation and (ii) lateral flow. In each grid cell, if melt takes place, the snowpack height is lowered by the amount of melt. We do not consider snow compaction, since on the scale of the snowpack height, the impact of intraseasonal snow and firn densification is likely negligible, especially when surface lowering due to melt is applied. If the snowpack is fully saturated according to a fixed irreducible water saturation threshold, then all residual meltwater percolates vertically into the lateral flow domain. Vertical meltwater percolation is assumed to occur "instantaneously", i.e. water that has percolated vertically can be transported laterally within the same timestep. The grid cell height either remains constant, or, when surface lowering due to melt is applied, decreases by the amount of melt in a specific grid cell at each timestep. We neglect precipitation inputs during the model run as they are usually negligible to small on the K-transect (Smeets and others, 2018). If refreezing is employed, the amount of superimposed ice (hereafter 'SI') formation is determined every timestep and this is also subtracted from the water table and grid cell height. Refreezing only takes place on the bottom surface of each cell, in the form of ice accreting on top of the underlying ice slab. The bottom of each grid cell is a no-flow boundary for meltwater with, in case of refreezing, a conductive heat flux that describes the temperature contrast between the sub-zero temperature of the ice slab and the grid cell temperature of 0∘C.

Lateral meltwater flow is calculated based on the hydraulic gradient between adjacent grid cells. No lateral inflow can take place in the uppermost grid cell of the model transect. The outflow of the grid cell at the lowest elevation along the transect is calculated based on the hydraulic gradient of the second-to-lowest grid cell, to avoid any artificial accumulation or accelerated drainage of meltwater at the end of the transect as a result of a changing hydraulic gradient. As soon as the water level equals the snowpack height in any one of the grid cells along the modelled transect (i.e. once the vertical percolation domain has been

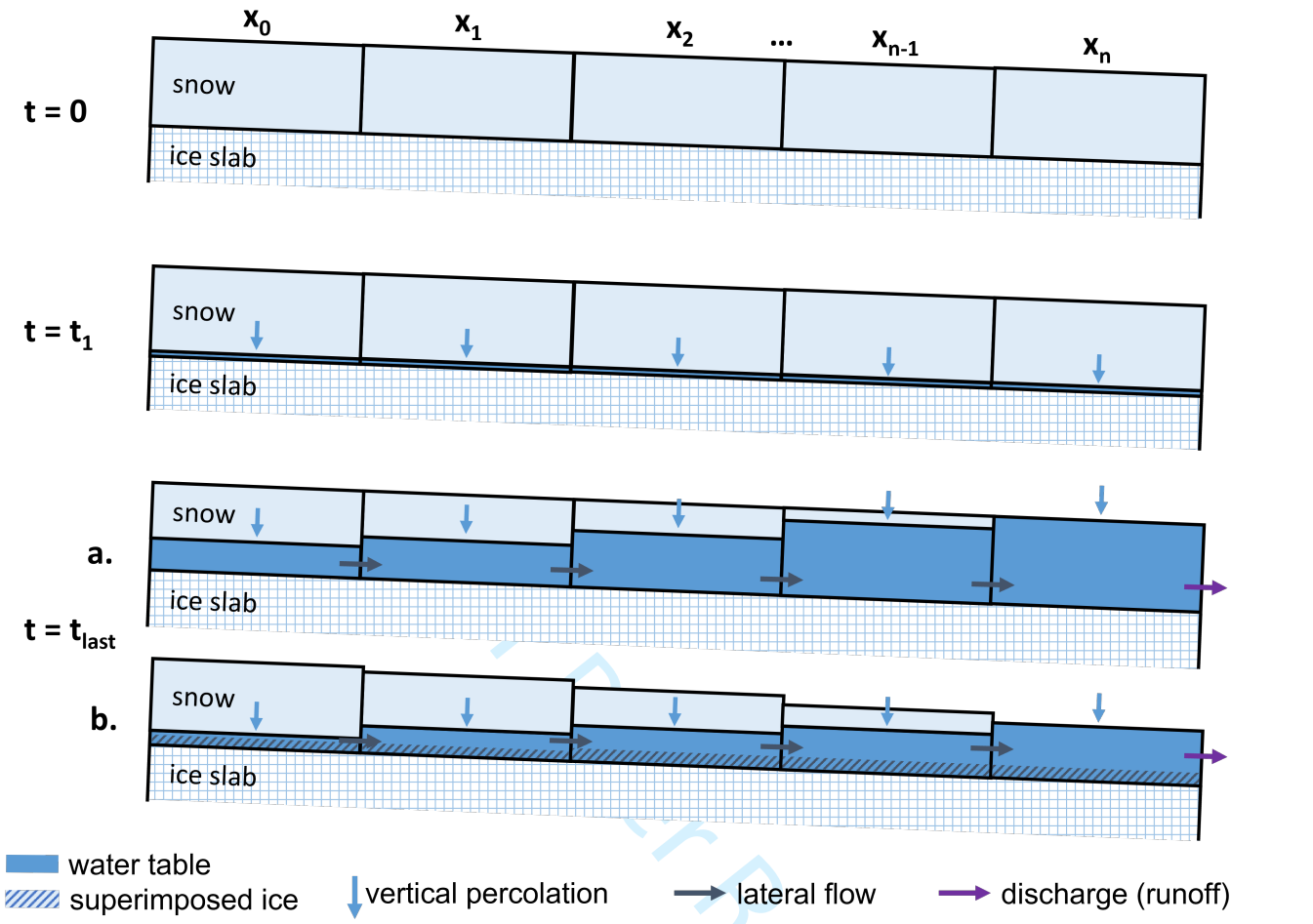

Fig. 1. Model schematic at three different time steps. For $t=t_0$ and $t=t_1$ no visible differences are present between the various modelling scenarios (t_1 being the first timestep in which melt occurs). For $t=t_{last}$ the two most extreme cases are displayed: (a) without surface lowering and refreezing, and (b) with surface lowering and superimposed ice formation.

removed by melt, or its pore space has been filled completely) the simulation is stopped, as surface runoff is not included in the model. Total discharge is the amount of water having flowed out of the lowermost grid cell of the modelled transect at the moment the model run ends.

We simulate a range of model scenarios consisting of conceptual sensitivity tests and empirically-driven runs which allow for qualitative comparison with field observations. The scenarios for the main, empirically-driven model runs are based on four melt summers (April 1st–October 1st for two warmer and two colder melt seasons), two slope types (a constant slope for sensitivity testing, and the K-transect slope for data-based simulations), three elevation ranges (1900-1700, 1900-1800 and 1800-1700 m a.s.l.), in- and excluding surface lowering by melt, and finally in- and excluding refreezing by SI formation.

Table 1 summarises the model parameters used in the main model runs. In the vertical percolation

Table 1. Values of the parameters used in this study

Description	Symbol	Value	Units
General			
Gravity constant	g	9.81	m s^{-2}
Ice density at -10∘C	ρ_i	918.9	kg m^{-3}
Fluid density of water at 0∘C	ρ_w	1000	kg m^{-3}
Dynamic viscosity of water	μ	$1.7916 \cdot 10^{-3}$	Pa·s
Snowpack porosity	ϕ	0.45	m^3 m^{-3}
Meltwater flow			
Lateral flow velocity	k_{lateral}	$1.92 \cdot 10^{-3}$	m s^{-1}
Irreducible water saturation	$S_{\text{w,irr}}$	0.01	m^3 m^{-3}
Hydraulic conductivity	K	0.384	m s^{-1}
Refreezing			
Heat capacity of ice	c_p	$2.0 \cdot 10^3$	J kg^{-1} K^{-1}
Thermal conductivity of ice	K_{therm}	2.30	W m^{-1} K^{-1}
Latent heat of freezing	L_{refr}	$3.34 \cdot 10^5$	J kg^{-1}
Ice slab surface temperature at 0 m depth	T_{slush}	0	∘C
Ice slab temperature at 2-10 m depth	T_{iceslab}	-10	∘C
Model properties			
Average ice slab surface slope		-0.005	m m^{-1}
Initial snowpack height	$h_{t=0}$	0.5 or 1.0	m w.e.
Grid cell width	dx	100	m
Transect length	l	13.6 to 28.6	km
Timestep	dt	3600	s

domain, the initial grid cell height or snowpack thickness ($h_{t=0}$) is set to either 1 m w.e. for the conceptual model runs with a constant slope, or reduced to 0.5 m w.e. for the empirical simulations to represent the relatively low amount of winter accumulation in this area.

In the lateral flow domain, for the slope of the transect we either use an averaged, spatially constant downhill slope equal to the average K-transect slope between 1900 and 1700 m a.s.l. (-0.005 m m^{-1}, or ∼5 m elevation loss over 1 km) or the actual slope along the K-transect according to the ArcticDEM (Porter and others, 2018) in the defined elevation range. Model transects have a length of 13 or 29 km depending on which elevation range is used, with a constant grid cell width of 100 m.

We impose the following hydrological parameters across the vertical and lateral flow domains. Average matrix porosity is set to 45%, following the field measurements described in Clerx and others (2022). We divide their observed average lateral meltwater flow velocity ($1.92 \cdot 10^{-3}$ m s^{-1}) by the average local surface slope from the ArcticDEM (-0.005 m m^{-1}) as the hydraulic gradient, to obtain the hydraulic conductivity of the slush matrix (0.384 m s^{-1}), assuming that the measured flow velocity equals the specific discharge in Eq. 3. Irreducible water saturation is set to 2% pore volume, which is the lower bound of $S_{w,irr}$ observed in the long-term drainage experiments in snow and firn by Denoth (1982).

At each timestep we calculate the snowpack height (thickness of the vertical percolation domain), water table height (thickness of the lateral flow domain), volume of water flowing into and out of both model domains, amount of SI formation and the resulting hydraulic gradient. All output is given in m w.e. To ensure model stability, grid cell dimensions need to be chosen such that the distance water can travel laterally in a single timestep is always smaller than the defined grid cell width. Furthermore, timesteps must be small enough to allow for instantaneous vertical percolation (i.e. hourly).

Meltwater input

Meltwater input for the simulations was obtained from the surface energy balance model (SEBM) described in van As (2011); van As and others (2012, 2017). The SEBM uses interpolated data from the weather stations along the K-transect and calibrated satellite-derived albedo data in an observation-based approach to calculate all surface mass- and energy fluxes in 100 m-surface elevation bins. We linearly interpolate the melt quantities provided by the SEBM over our modelled elevation range to calculate the amount of melt experienced in individual grid cells throughout the four modelled melt seasons. Liquid water supplied to the snowpack by rainfall or condensation is assumed negligible and not included in our model runs.

To investigate the impact of varying melt season characteristics, we selected four years with distinctly different melt patterns: 2012 and 2019, classified as “warm” or “high-melt” years, and 2017 and 2020, categorized as “cold” or “low-melt” years. Apart from variations in the total supplied meltwater each year, all years show a distinct temporal evolution of the melt season. Figure 2 illustrates these differences. In 2012, early melt peaks were observed in June, whereas 2019 featured a later and more gradual development of meltwater supply. Likewise, in 2017 there was a major melt event during mid-late August, in contrast to 2020 when the melt season evolved more gradually. Note that the total cumulative melt along the K-transect in 2019 is relatively low compared to 2012, but according to GRACE and other mass balance

measurements it was a large mass loss-year Greenland-wide (Tedesco and Fettweis, 2020). Furthermore, the maximum elevation of the visible runoff limit in 2019 (1822 m a.s.l.) was comparable to the the record year of 2012 (1841 m a.s.l.). In 2017 and 2020 the visible runoff limit was identified at lower altitudes, at 1663 and 1708 m a.s.l. respectively (Machguth and others, 2022).

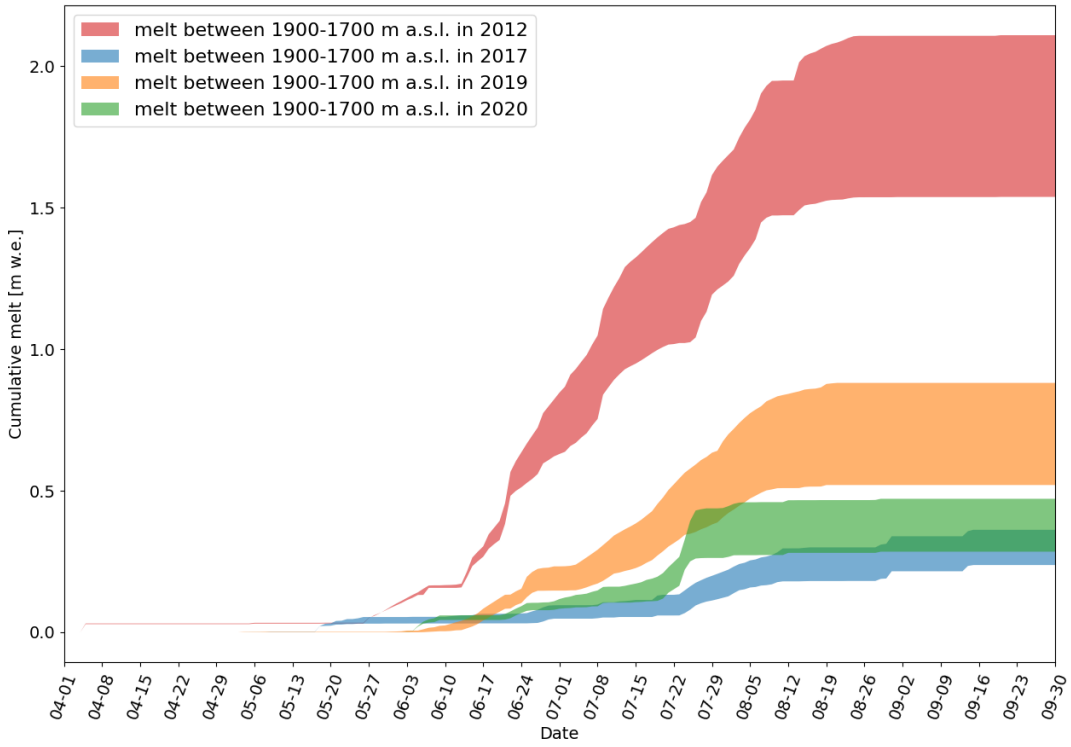

Fig. 2. Cumulative melt over time for the four melt seasons along the K-transect (67◦N, 47◦W) used as input for simulations. Shaded areas indicate the cumulative melt between 1700 m a.s.l. (upper limit of all shaded areas) and 1900 m a.s.l. (lower limit of all shaded areas) according to the SEBM.

Refreezing

Refreezing is the freezing of liquid water delivered to the glacier surface (i.e. meltwater generated in situ, or rain) having percolated to some depth (Cogley and others, 2011). Meltwater infiltration and refreezing processes are dependent on the timing and quantity of meltwater input and initial temperature conditions (Pfeffer and Humphrey, 1998). Cogley and others (2011) specify that "when refreezing occurs below the previous summer's surface it represents internal accumulation, when it occurs at the base of snow overlying impermeable glacier ice it is called superimposed ice" (SI). However, since summer surfaces are hard to reliably locate in the accumulation zone of the Greenland ice sheet and are not relevant in our minimalistic

model approach, we consider all refreezing to result in SI and do not distinguish between SI formation and internal accumulation. Our definition of SI hence bears more resemblance to the term infiltration ice, meaning ice derived from the refreezing of meltwater having filled up snow- or firn porosity (Shumskii, 1964).

In our model an isothermal snow layer overlies the ice slab which initially has a subfreezing temperature. Meltwater which is present on top of the ice slab refreezes onto the slab based on the 1D heat equation:

$$\frac{\partial T}{\partial t} = \frac{K_{therm}}{\rho c_p} \frac{\partial^2 T}{\partial z^2} \tag{1}$$

where T is the ice slab temperature [∘C], K_{therm} is the ice thermal conductivity [W m^{-1} K^{-1}], ρ the ice slab density [kg m^{-3}] and c_p the specific heat capacity of ice at -10∘C [J kg^{-1} K^{-1}]. The temperature change $\frac{\partial T}{\partial t}$ [∘C s^{-1}] determines the amount of refreezing Δz [m w.e.] that can take place in each time step following:

$$\Delta z = \frac{\rho c_p}{L_{refr}} \left(\frac{\partial T}{\partial t} * \Delta t \right) \tag{2}$$

with L_{refr} the latent heat of freezing [J kg^{-1}] and Δt the timestep length [s].

Here, we implement refreezing onto the ice slab using an offline forward Euler scheme that solves the 1D heat equation. This scheme provides a look-up table of SI formation as a function of time elapsed since the first timestep at which meltwater percolated down to the ice slab, i.e. entered the lateral flow domain. It models refreezing by assuming an ice slab thickness of 10 m, with an initial ice slab temperature gradient decreasing linearly from 0∘C at the slab surface to -10∘C at 2 m depth, and then a constant temperature of -10∘C to 10 m depth. This initial temperature gradient is broadly representative of in-situ temperature profiles around the time when the snowpack becomes isothermal as a result of melting and vertical percolation.

We run the refreezing scheme under the assumption that liquid water is always available on the ice slab surface for refreezing. At each timestep this yields the change in the ice slab temperature profile and the maximum amount of refreezing that can take place. During model runs that incorporate refreezing, we use this output to determine refreezing in each grid cell as a function of both the time elapsed since the cell's snowpack became isothermal and the amount of water available for refreezing. Meltwater that refreezes is removed from the water table, and any remaining meltwater percolates laterally.

Lateral meltwater flow

Darcy's law is an empirical equation describing the flow of a fluid through a porous medium. It relates the flow rate of the fluid to the hydraulic gradient:

$$q = \frac{Q}{A} = -K\frac{dh}{dx} \tag{3}$$

where q is the specific discharge, sometimes also called Darcy velocity [m s^{-1}], Q is the flow rate or total discharge [m^3 s^{-1}], $\frac{dh}{dx}$ is the hydraulic gradient [m m^{-1}], A is the area through which flow occurs [m^2] and K the hydraulic conductivity [m s^{-1}].

The hydraulic head h is a measure of fluid potential, or otherwise said the liquid pressure above a certain datum. It is the sum of two components: the elevation head z and the pressure head Ψ. Given that we are dealing with a single fluid, water, in an unpressurised system (where grid cells are open to the atmosphere), the pressure head is constant everywhere and the fluid potential is solely a result of the water table height and topographical elevation. Consequently, the hydraulic head can be simplified to the elevation head z. The hydraulic gradient is the difference in hydraulic head over the length of the flow path, which in this case is the distance between adjacent grid cells.

The hydraulic conductivity K describes the ease with which a fluid can move through a porous medium. It depends on the intrinsic permeability of the medium, the degree of fluid saturation, and the density and viscosity of the fluid, and is defined as:

$$K = \frac{k\rho g}{\mu} \tag{4}$$

with k being the matrix permeability [m^2], and ρ and μ the density [kg m^{-3}] and dynamic viscosity of the fluid [Pa·s].

Assessing model sensitivity

To determine the sensitivity of the model to the main input parameters, we conducted a sensitivity study using a model transect with a linear slope between 1900 and 1700 m a.s.l. We focused on three parameters with considerable uncertainty: hydraulic conductivity K, irreducible water saturation $S_{\mathrm{w,irr}}$, and initial snowpack height h. Other input parameters, such as snowpack porosity, ice slab temperature gradient, and surface slope either exert a smaller influence on the modelling results, or manifest their impact on the simulation indirectly through the selected modelling approach for the empirically-driven model runs.

Table 2. Low, base and high case values of parameters used for sensitivity analysis.

	Low	Base	High	Unit
K	$7.22{\cdot}10^{-2}$	$3.84{\cdot}10^{-1}$	$7.88{\cdot}10^{-1}$	m s^{-1}
$S_{w,irr}$	-	0.01	0.07	m^3 m^{-3}
$h_{t=0}$	0.3	1.0	2.0	m w.e.

Table 2 shows the low, base, and high case values for the three tested parameters. For K, the chosen low and high case estimates correspond to the minimum and maximum observed lateral flow velocities in Clerx and others (2022) divided by the slope of the study area, as the base assumption considers their average measured velocity. Further examination of why these values were chosen and how uncertain K is can be found in the discussion.

The base case of $S_{w,irr}$ was set to 2% of the pore volume, which roughly equals 0.01 of the total volume, the minimum observed value by Denoth (1982). This value was chosen as to limit the impact of this parameter on lateral meltwater flow in the model, resulting in this parameter only having a base- and high case in the sensitivity study. The high case value for $S_{w,irr}$ was set to 15% pore volume, or roughly 0.07 of the total volume, which is the highest value measured by Denoth (1982) in a snow type that is still somewhat similar to the observed slush matrix.

Considering $h_{t=0}$, the base case assumption of 1 m w.e. for the simulations over a linear slope is a slight overestimation of the annual accumulation in the study area. However, this choice was deliberate, as the main purpose of the model is to evaluate water table evolution over time, as well as over substantial lateral distances. Lower $h_{t=0}$ would lead to very short simulations, since meltwater would appear at the surface as a result of the complete snowpack melting away after only limited amounts of melt. This would render the modelling results less useful, as meltwater runoff generally occurs throughout prolonged periods and not only in the early summer months. For sensitivity testing, the low case $h_{t=0}$ corresponds to the average annual accumulation around KAN_U, whereas the high case value was set to 2.0 m w.e. Any higher $h_{t=0}$ would only occur in areas where, instead of ice slabs, firn aquifers form in the shallow subsurface.

To assess the model's sensitivity to changing these parameters we calculated three metrics. (i) Normalised discharge [m w.e.] corresponds to the total discharge (meltwater leaving the bottommost grid cell) divided by the average total supplied meltwater per grid cell in each model run. (ii) Simulation length describes the number of days before the water table completely saturates the snowpack in any one of the grid cells. (iii) Total SI formation is the volume of water [m w.e.] that is refrozen onto the ice slab along

the full model transect throughout the complete duration of the model run.

RESULTS

Model sensitivity

Figure 3 shows three tornado plots that depict variations from the base case when using different values for hydraulic conductivity, irreducible water saturation, and initial snowpack height for each of these metrics. Hydraulic conductivity K has a relatively symmetrical effect on how much water leaves the model (Fig. 3a). The influence of irreducible water saturation $S_{w,irr}$ is very limited, whereas variations in initial snowpack height $h_{t=0}$ have a considerable positive and negative impact in warm and cold melt seasons, respectively. The model simulation length (Fig. 3b) is predominantly influenced by $h_{t=0}$: despite the relatively high lateral meltwater flow velocities the amount of snowpack available to accommodate melt is the most important parameter determining when water occurs at the snow surface. The amount of SI formation (Fig. 3c) represents the amount of meltwater retention and shows that the relatively conservative value for $S_{w,irr}$ could result in underestimation of SI formation. Initial snowpack height $h_{t=0}$ is once again the most influential parameter, and variations in K have less impact on the amount of SI formed.

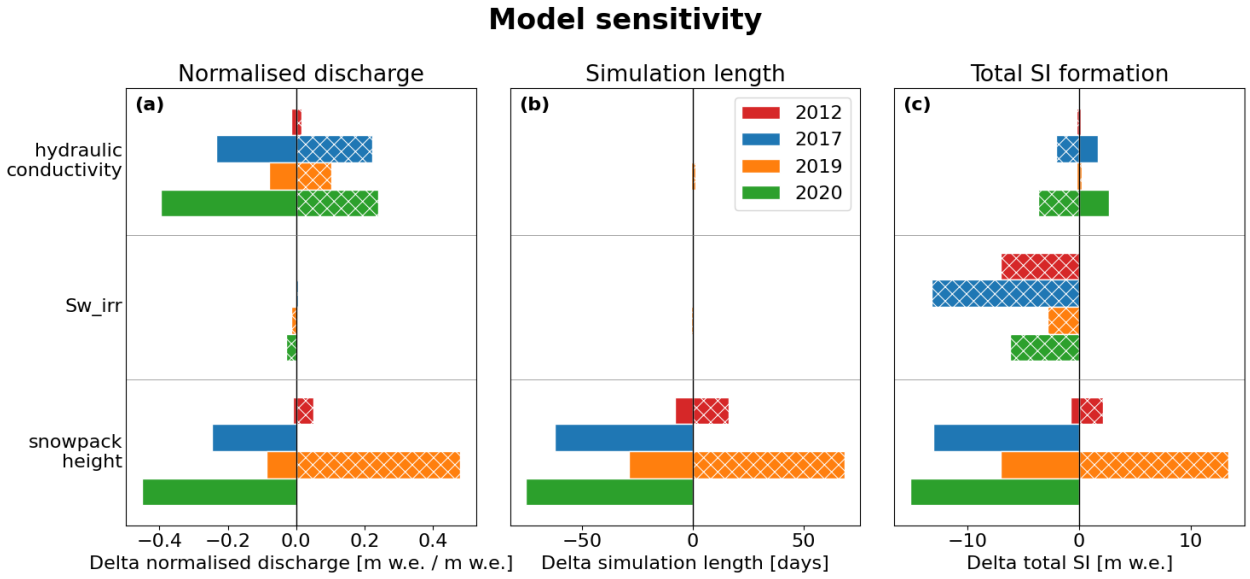

Fig. 3. Tornado plots showing model sensitivity to hydraulic conductivity, irreducible water saturation and snowpack height, displayed by variations in (a) normalised discharge, (b) simulation length, and (c) total volume of SI at the end of each simulation. Hashed bars indicate the effect of using the high case of each tested variable, solid bars show the results when using the variable's low case.

The sensitivity study highlights the generally astute selection of the chosen base case values. Nonethe-

less, certain parameters, notably snowpack height, exert a pronounced influence on the model results.

Simulations along a linear slope

Figure 4 shows the evolution of water table height (a and b), snowpack height (c) and SI formation (d) during the 2020 melt season along a transect from 1900-1700 m a.s.l. with a linear slope, ∼29 km in length. Panels (a) and (b) illustrate that the maximum water table height reached during the summer of 2020 was determined principally by the amount of melt input, and that SI formation plays a minor role. When comparing panels (a) and (b), two effects of SI formation are visible. Firstly, SI formation leads to a reduction in the maximum water table height (0.41 vs. 0.35 m w.e. early August), and secondly it curtails the build-up of a water table at higher elevations, resulting in a diminished volume of liquid water present at the end of the melt season (maximum water table height of 0.33 vs. 0.23 m w.e. end September). Moreover, liquid water persists longer and further downslope at the end of the melt season when SI formation occurs, indicated by the presence of water from about 15 km along the transect onwards in (b), whereas the water table is present below around 13 km in (a) at the end of September. This is mainly a result of the longer model runtime: applying surface lowering and SI formation reduces the maximum water table height preventing the early occurrence of water breakthrough, which provides more time for the meltwater to move downslope.

Figure 5 shows characteristics of the simulation results for all of the four selected melt seasons, along the same transect as used for Fig. 4. We computed normalised discharge and SI volume as fractions of the total available meltwater per grid cell in each model run at the end of the simulation. Given that some simulations do not run until the end of the simulation period (1 October) because the slush limit appears throughout the melt season, the absolute volume of meltwater discharge or water retained as SI cannot be compared quantitatively. The normalised values given here hence provide a way of removing the impact of the varying simulation lengths, as they only take into account the quantity of meltwater that was available during the model run, and not the total amount of melt throughout the whole melt season.

Results show that water surfaced early in the season for 2012 and in two out of three cases for 2019, as a result of the high amount of meltwater input in these years. Although the total cumulative melt in 2019 was less than 1 m w.e., the visible runoff limit appeared around end July. In 2012, this amount of melt was already reached before mid July (see also Fig. 2), accompanied by meltwater appearing at the surface before the end of June.

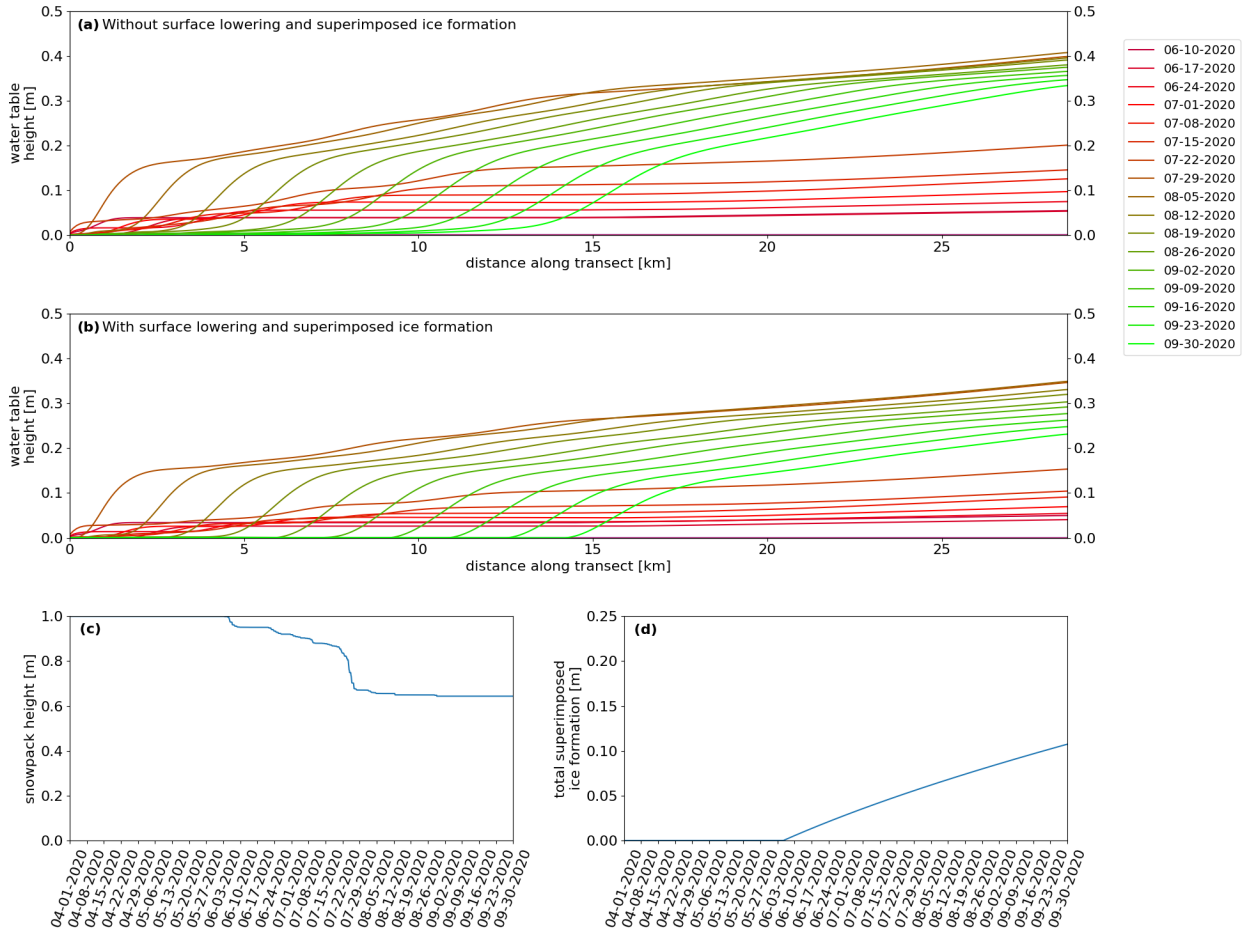

Fig. 4. Water table evolution for the 2020 model runs (a) excluding and (b) including surface lowering and SI formation. Every coloured line represents the water table height at a weekly interval after the initial occurrence of water in the lateral flow domain. For the latter scenario snowpack height (c) and cumulative SI formation (d) are shown for a grid cell in the middle of the transect, at 1800 m a.s.l.

The earlier in the melt season the water breakthrough, the more water is still present in the system, due to the fact that there has been less time for evacuating water. This is shown by the lower values for normalised discharge in 2012 than in 2019 when looking at cases without SI formation. Much of this water presumably continues to drain out of the slush and into river channels which incise headwards after meltwater breakthrough, but simulating surface meltwater runoff is not included in the current modelling set-up.

Surface lowering has a stronger effect on the occurrence of the visible runoff limit than SI formation: the amounts of SI formed are an order of magnitude smaller than the surface height reduction by melt (e.g. 0.05 vs. 0.5 m w.e. for 2019; Fig. 5b and c). SI formation, however, can reduce the total amount of runoff by up to almost half: in 2012, normalised discharge is reduced to 6% with SI formation vs. 10% without

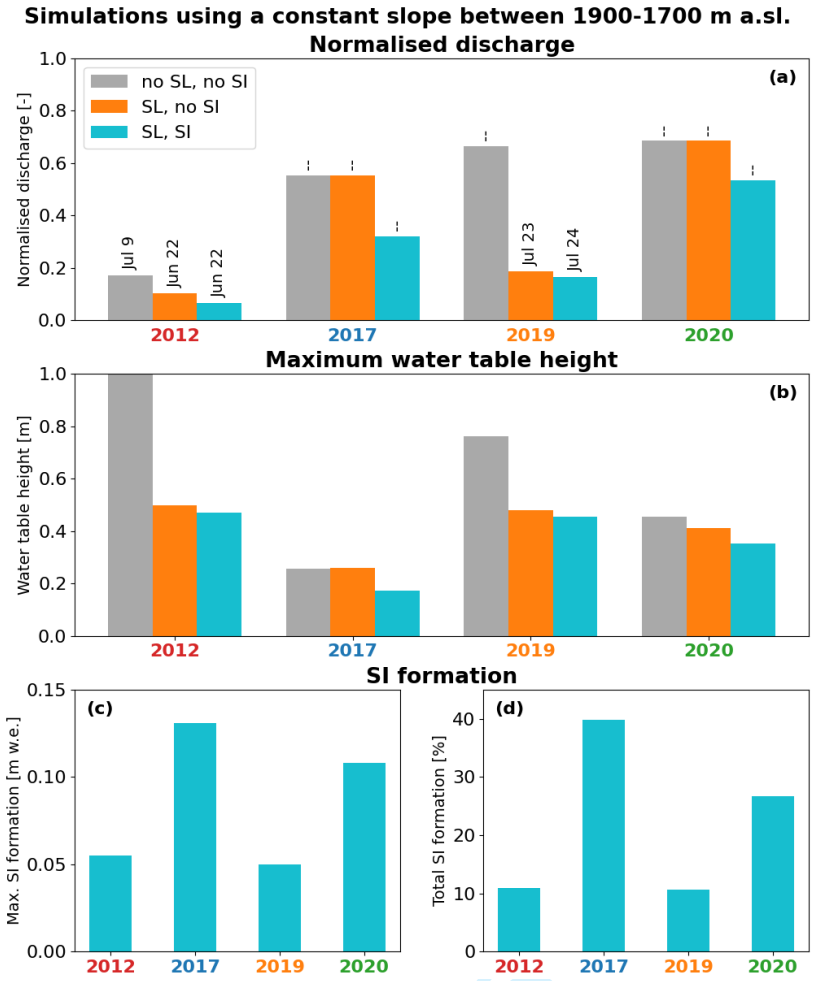

Fig. 5. Simulation results for modelling runs along a transect with a constant slope between 1900-1700 m a.s.l. for four different melt seasons. SL and SI stand for surface lowering (due to melt) and superimposed ice formation, respectively. Panel (a) shows normalised discharge, with bar labels indicating the water breakthrough date (i.e. simulation length). In panel (b), the maximum water table height attained during the model run is displayed. Panel (c) shows the maximum height of SI formed in individual grid cells, and panels (d) and (h) displays the total amount of SI formed along the full model transect as a percentage of the total meltwater available in the whole model run.

SI formation (Fig. 5a).

Simulations along the K-transect

Figure 6 shows the water table height (solid lines) and snowpack thickness (dashed lines) for the 2019 (warm; panel a) and 2020 (cold; panel b) melt seasons along a transect with the actual surface slope around the weather station KAN_U following the ArcticDEM, for the case where both surface lowering and SI formation were applied. Note the significant scale difference between the x- and y-axis in Fig. 6c: the x-axis shows the horizontal distance of almost 30 km, whereas the y-axis displays the total elevation difference which is only 200 m. The initial snowpack height for these model runs was a more realistic

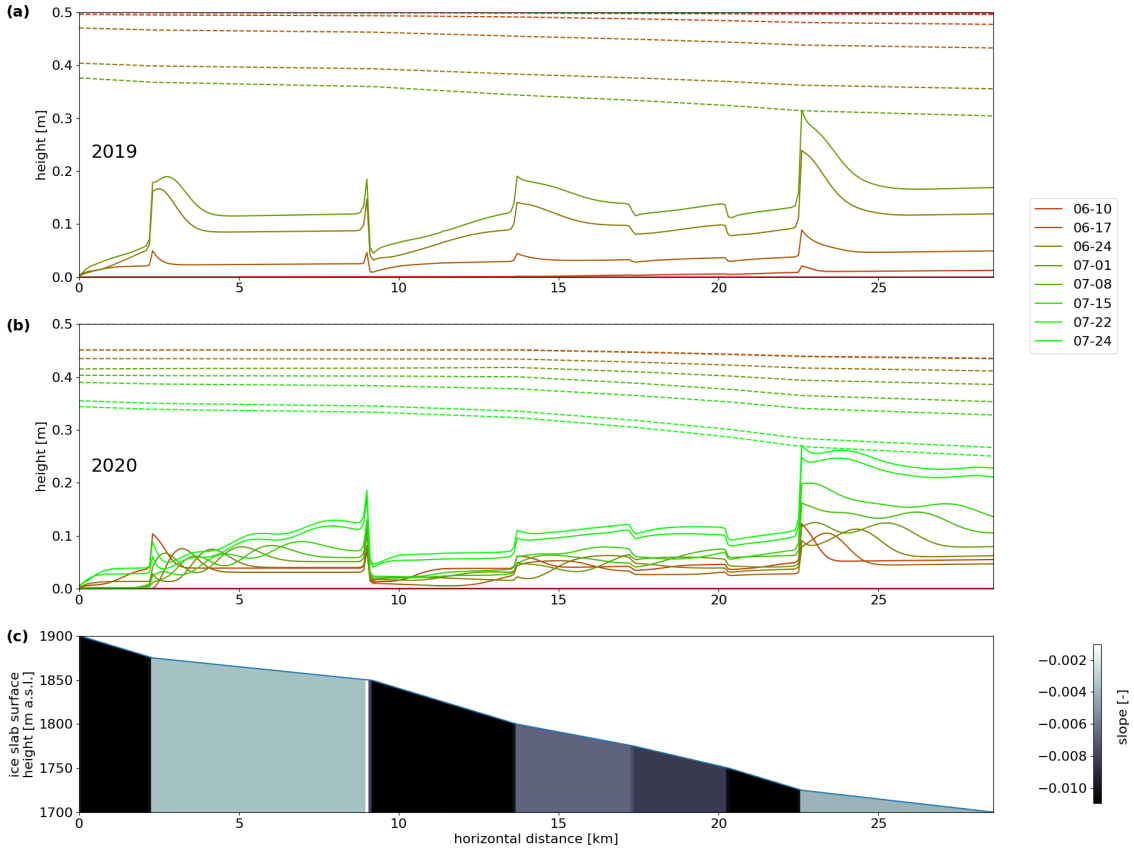

Fig. 6. Evolution of water table (solid) and snowpack (dashed) height over time for 2019 (a) and 2020 (b) with surface lowering and SI formation, and (c) grid cell height and slope gradient along the transect. Every coloured line represents a weekly interval after the initial occurrence of water in the lateral flow domain. Absent lines in 2019 (a) are a result of the simulation being stopped due to earlier water breakthrough than in 2020. Note the small area of zero-slope around 9 km along the transect.

366 0.5 m w.e. as opposed to the 1 m w.e. initial snow thickness for the reference runs described in the
367 previous section. Logically, reducing the snowpack thickness to 0.5 m w.e. has a significant impact on the
368 model run duration: the water table now reaches the surface in all model runs except for the simulation
369 for 2017 along the 1900-1800 m a.s.l. transect (Fig. 7a).

370 Changes in transect gradient have an important effect on the water table height. Both in Fig. 6a and b
371 it can be seen that at 2 km, just before 9 km and around 14 and 23 km water accumulates due to a slope
372 decrease, whereas at 9 km, 17 km and just after 20 km water is evacuated more efficiently, demonstrated
373 by a local decrease in water table height related to an increase in slope.

374 Especially in 2020 (Fig. 6b) the effect of lateral meltwater flow is clearly visible by the downslope
375 migration over time of the highest water table below 2 km and 22 km, where the transect slope decreases.
376 Similarly, in 2019 (Fig. 6a) the water table peak around 2 km moves slightly downslope after a short pause

in meltwater supply between the 1st and 8th of July.

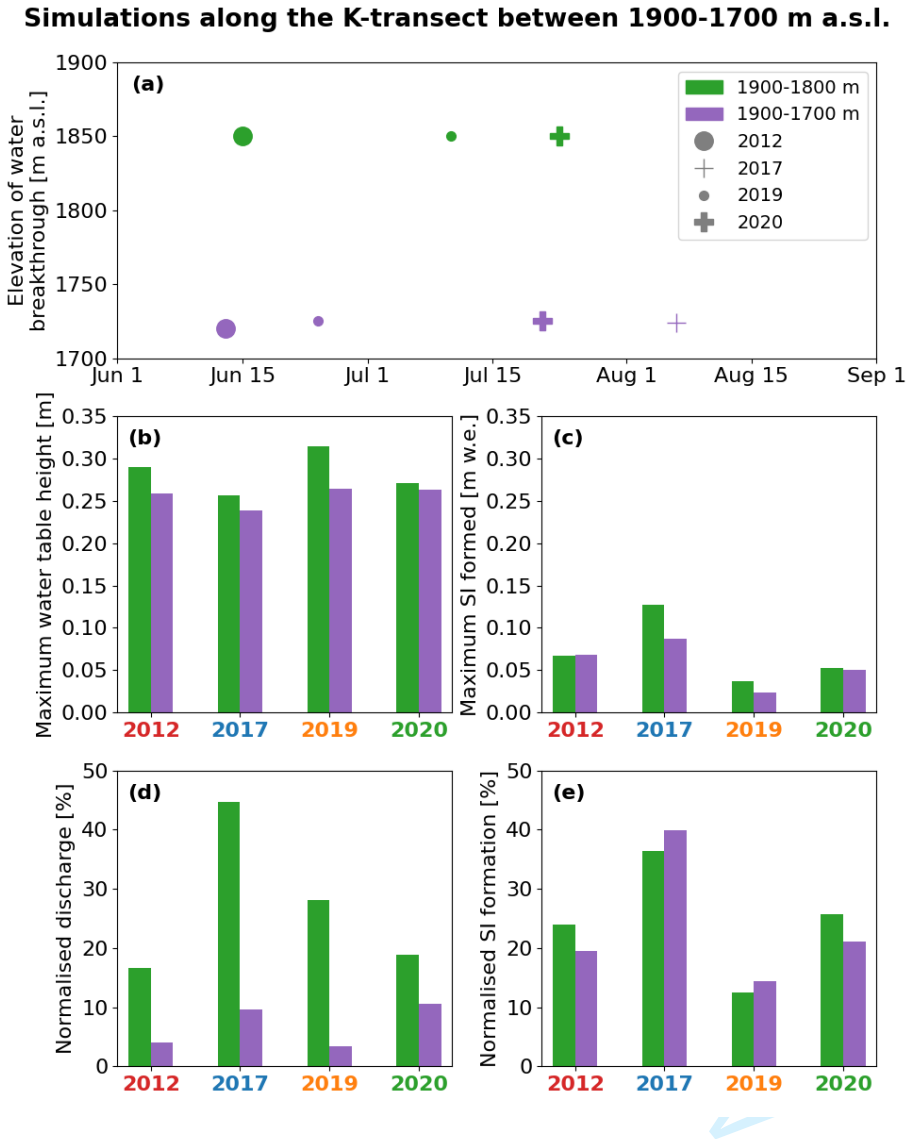

Fig. 7. Simulation results for modelling runs along the K-transect slope between 1900-1700 m a.s.l. and 1900-1800 m a.s.l. for four different melt seasons, with surface lowering due to melt and SI formation. Panel (a) shows the elevation and date at which meltwater appears at the surface. In panel (b), the maximum simulated water table height reached is shown. Panel (c) displays the maximum height of SI formed throughout the melt season. Panels (d) and (e) show the total amount of discharge and SI formation as a percentage of the total meltwater available in the whole model run.

Figure 7 shows the results for the simulations along the K-transect slope displayed in Fig. 6c for all studied melt seasons, for a transect between 1900-1800 m a.s.l. (green bars) and for the transect spanning the full elevation range (1900-1700 m a.s.l.; purple bars) to investigate the impact of less melt at higher elevations. In all these model runs the initial snowpack height was 0.5 m w.e.

As shown in Fig. 7a, both transects have a specific elevation for water breakthrough at the surface,

regardless of its timing, corresponding to an inflection point in surface slope. In general, the maximum water table reached is slightly higher for the shorter (1900-1800 m a.s.l.) transect (Fig. 7b). Similarly, when only looking at the upper part of the transect (green bars), there is 2-5% more accretion of SI in individual grid cells than when considering the 1900-1700 m a.s.l. elevation range (purple bars; Fig. 7c). The discharge as a function of total meltwater available during the model run (Fig. 7d) is substantially higher for the shorter model transect (green bars). These results are primarily a function of the model's longer runtime before the visible runoff limit appears in case of the model runs using the 1900-1700 m a.s.l. transect. The total thickness of newly formed SI as a function of the amount of meltwater available throughout the whole melt season is similar across the two transect variations (Fig. 7e).

DISCUSSION

Timing and location of slush appearance

As shown in the sensitivity analysis (Fig. 3), initial snowpack height $h_{t=0}$ plays an important role in the timing of slush appearance at the surface, even within the narrow yet realistic range of minimum and maximum values. The chosen initial snowpack height exceeds measured values, in particular for the model runs over a linear slope, but using more realistic, lower values reduces model utility as water breakthrough occurs earlier, stopping the model run.

The increase in water table height over time on top of an ice slab is dependent on the evolution of the melt season throughout the summer. Shorter, intense periods of melt are more likely to cause the appearance of visible runoff than more gradual meltwater supply, as shorter periods allow for less lateral flow through the firn evacuating the meltwater downslope.

In general, the occurrence of visible runoff takes place later in the melt season at higher elevations according to the results for the two modelled elevation intervals (Fig. 7a): simulations using the longer 1900-1700 m a.s.l. transect (purple markers) result in earlier occurrence of the slush limit than on the shorter transect. This is a result of the lower amount of melt at higher elevations, as well as the impact of lateral meltwater supply. For 2012 and 2020 there is relatively little difference in timing between the two elevation ranges due to the rather abrupt, large melt events taking place towards the end of June in 2012 and late July in 2020, but for 2017 and 2019 there are significant delays in slush limit occurrence between the transect from 1900-1800 m a.s.l. when compared to 1800-1700 m a.s.l. results. Abrupt and strong melting seems to lead to flooding of the snowpack over substantial elevation intervals, whereas sustained,

moderate melt does not have this effect.

In colder summers, when the simulated water table does not reach the snow surface, differences in the total amount of discharge and SI formation are principally due to differences in temporal evolution and the total quantity of meltwater generated during the melt season. For example, in 2017 more SI was formed because of a more gradual evolution of the melt season, whereas in 2020, when a big melt event occurred in late July, a larger part of the supplied meltwater ran off. Apart from the higher absolute amount of liquid water available in 2020, there was less time for refreezing that year due to the sudden input of melt and subsequent faster lateral meltwater displacement as a result of higher hydraulic gradients.

When comparing the characteristics of the linear model runs to those of the runs with a varying slope along the K-transect, it can be seen that the influence of slope variations is larger than that of surface lowering: for the same melt input, the water table reached higher levels more rapidly when the transect followed a non-linear slope (Fig. 5a and Fig. 7a, purple markers). In the simulations with a linear slope, the maximum water table attained at the end of the simulations was approximately half the initial snowpack height of 1 m w.e. but smaller in most cases (Fig. 5b). For the model runs using the K-transect slope, the maximum water table height at the time of water breakthrough was roughly 0.6x the initial snowpack height of 0.5 m w.e (Fig. 7b). Across all simulations along the K-transect elevation profile, meltwater first occurred at locations characterised by a decrease in slope. This is particularly pronounced during colder summers with a gradual supply of meltwater, when lateral flow is of even greater relative importance for total runoff than when short-lived, intense melting provides the majority of liquid water. Changes in ice slab slope, or more broadly in surface slope, therefore play a major role in the occurrence of the visible runoff limit.

Our results corroborate with the findings on the daily variation of visible runoff limits by Machguth and others (2022) for the four melt seasons studied here. In particular in the simulations for the 100 m elevation transect (Fig. 7a, green markers), the timing of meltwater appearing at the surface roughly corresponds to when the maximum visible runoff limit was observed on satellite imagery. However, a comprehensive comparison with field observations remains challenging due to the simple nature of the lateral flow model. In the current model configuration, meltwater is only transported downslope, and each grid cell can only receive meltwater input from its upslope neighbour. In reality, flowpaths are a function of the surface hydrological catchment, so a given point in space could receive meltwater input from several directions.

At present, simulations are stopped as soon as the water table height reaches the snow surface in any of

the grid cells, since surface meltwater runoff is not included in the model. This is the most obvious (or only physically realistic) end for a model run currently. We have only very limited knowledge on how fast water flows in slush fields, or how these develop into efficient supraglacial drainage systems (e.g. Holmes, 1955). From satellite imagery it is clear that, after a certain period of time with sufficient and sustained melt, slush fields nearly always transition into more confined supraglacial river systems. Given the efficiency of this process – based on remote sensing data we can observe that the development of efficient surface drainage systems is a matter of days rather than weeks, including a simplistic bucket scheme in the model for surface runoff would probably be a valid approximation. This would avoid the necessity of incorporating a full 2D-meltwater routing scheme with all related assumptions and uncertainties. Ideally, the model should always run until the end of the melt season regardless of the amount of melt to allow for adequate comparison between individual melt seasons. Including surface runoff, even in the form of a simplistic bucket scheme, would allow simulations to run for the full melt season.

Lateral meltwater runoff and hydraulic properties

Lateral meltwater runoff is highly efficient in all model simulations. For any grid cell except the uppermost along the transect, runoff greatly exceeds the amount of vertical surface meltwater input due to the large lateral inflow from higher elevations. Depending on the temporal evolution of the melt season, total lateral runoff is roughly 40 times the average meltwater input per grid cell at the time the water table reaches the snow surface. The amount of lateral runoff as a function of average total meltwater generated in grid cell is higher for the 1900-1800 m a.s.l. transect than for the transect spanning a 200 m-elevation range (56x vs. 37x more runoff than melt input, respectively).

The model outcomes from the longer transect show lower values for the normalised discharge (Fig. 7d; green bars). This is due to the fact that it takes much longer for meltwater to exit the transect as the model grid is about twice as long as that of the transect spanning a 100 m elevation range.

The sensitivity study shows that the hydraulic conductivity has a large impact on the model results, in particular concerning the amount of meltwater discharge and retention. Measured hydraulic conductivities of firn at various glaciers across the world fall within a relatively narrow range, typically between $1{\cdot}10^{-5}$ and $5{\cdot}10^{-5}$ m s^{-1} (Fountain and Walder, 1998). However, in areas where firn aquifers exist, firn hydraulic conductivity measurements show a considerably wider range, spanning from $2.5{\cdot}10^{-5}$ to $1.1{\cdot}10^{-3}$ m s^{-1} (Miller and others, 2017), and when including measurements of weathering crust hydraulic conductivity ($3.47{\cdot}10^{-8}$

to $4.07{\cdot}10^{-5}$ m s^{-1}) this range widens further(Stevens and others, 2018). In the southwest of Greenland, hydraulic conductivity of near-surface icy firn has been measured at $2.4{\pm}1.0{\cdot}10^{-3}$ m s^{-1} (Clerx and others, 2022).

When calculating the hydraulic conductivity of the slush matrix using the Kozeny-Carman approximation for permeability of a porous medium consisting of perfect spheres (Kozeny, 1927; Carman, 1937; Bear, 1972), a more theoretical approach, using a porosity ϕ of 0.45, density ρ_w of 1000 kg m^{-3} and viscosity μ of $1.7916 \cdot 10^{-3}$ Pa·s (for water at 0∘C) yields a hydraulic conductivity of $3.67{\cdot}10^{-2}$ m s^{-1}. Using Calonne's and Shimizu's parametrisations for snow permeability, respectively (Calonne and others, 2012; Shimizu, 1970), in combination with the same parameters described for the Kozeny-Carman approximation, leads to theoretical values for hydraulic conductivity of $9.34{\cdot}10^{-2}$ and $3.30{\cdot}10^{-2}$ m s^{-1}.

In our model calculations, the hydraulic conductivity parameter K ($3.84{\cdot}10^{-1}$ m s^{-1}, which is two orders of magnitude higher than values measured in the laboratory-type experiments using icy firn by Clerx and others, 2022) is derived from observed lateral flow velocities of meltwater through slush, and not a direct material property measurement.

All in all, in the various measurements and possible theoretical approaches there is a spread of several orders of magnitude and hence substantial uncertainty in the hydraulic conductivity of snow and firn, with theoretical approximations giving values that are approximately in the middle of the range, and hydraulic conductivities measured in the field providing both lower and higher values. The currently used value for K in the model based on the field observations by Clerx and others (2022), was chosen in order to obtain modelling results that resemble in situ measurements of lateral meltwater flow. A lower hydraulic conductivity would lead to less runoff and a delay in occurrence of the visible runoff limit. For future model development, it is essential to better constrain the parameter space of potential hydraulic conductivity values by further in situ measurements of snow, firn and slush matrix hydraulic conductivity. Additionally, understanding how these values fluctuate throughout the melt season would be very valuable, as hydraulic conductivity is unlikely to remain constant as a result of meltwater processes and continued snow transformation.

The irreducible water saturation $S_{w,irr}$ is set to a relatively low value of 2% of the pore volume (∼0.01 of the total volume) in our simulations, to reduce the importance of the vertical flow domain in the model. We do not have detailed insights into the actual residual water saturation in slush on top of ice slabs. Furthermore, considerable uncertainty remains in general as to what is a representative value for the

irreducible water saturation in snow. Dielectric measurements (Lemmelä, 1973) show irreducible water saturations of 0.02-0.03 for a seasonal snowpack, whereas Coléou and Lesaffre (1998) measured values for wet snow between 0.05-0.15 in a laboratory setting. We consider the lowest value for $S_{w,irr}$ as reasonable, given the relatively high percolation- and lateral flow velocities compared to the model timestep, but also since large areas can undergo the transformation into slush fields within several days. Given the sensitivity of the ratio between meltwater runoff and retention (normalised discharge and SI formation in the sensitivity study) to irreducible water saturation, deliberate choices and further analysis of the most appropriate base case value for $S_{w,irr}$ should be made when developing the lateral flow model further.

Refreezing

Superimposed ice formation can account for meltwater retention of up to 40%, especially at high elevations (Fig. 7e). In case of intermittent melt pulses this can drastically delay or even completely inhibit the occurrence of visible water at the surface. Values for total thickness of newly formed SI as a function of total available meltwater are slightly higher for the upper (short) K-transect model runs as melt is slightly less at higher altitudes, resulting in a somewhat larger fraction of meltwater retention.

Simulated values for SI formation on top of the ice slab (0.02-0.13 m w.e.) are in rough agreement with data from Rennermalm and others (2021) when evaluating ice slab growth at KAN_U in consecutive years. Their firn cores yield values in the order of 0.3-0.4 m accretion of ice slab thickness per year (approx. 1.6 m ice in 5 years, or 0.28-0.37 m w.e. per year). The lower ice accumulation in the model is presumably a result of its 1D-nature only considering meltwater inflow from one direction, whereas in reality more water can accumulate due to local ice slab topography and resulting meltwater ponding.

In the current model configuration, refreezing only takes place in the lateral flow domain. This is a simplification, as we know from literature and field observations that ice lenses and glands form in the percolation domain (e.g. Baird, 1952; Koerner, 1970; Mikhalenko, 1989; Obleitner and Lehning, 2004; Parry and others, 2007; Cox and others, 2015), but deemed appropriate given the model simplicity and purpose. In other regions of the Greenland ice sheet, where crevasses and fractures are more common than in our study area, crevassing can increase the effective permeability enough to restrict lateral forcing and runoff, hence enabling enhanced refreezing of meltwater that vertically percolates to depth (Culberg and others, 2022). Additionally, refreezing can also occur from above (i.e. at the snow surface) and not only in the form of SI that accretes to the top of the ice slab.

At the start of all the model runs on April 1st, we assume that the full snowpack on top of the ice slab is isothermal at 0◦C, as we do not simulate the initial warming of the snowpack in the beginning of the melt season. Additionally, we do not model the vertical percolation domain in detail. In years characterised by low amounts of melt, this simplification does not fully capture refreezing processes, especially regarding the formation of ice lenses and intermediate refreezing that may have an impact on the flow properties of the snowpack. These assumptions hence may lead to an overestimation of SI formation in our model. However, the applied initial ice slab temperature gradient, where ice slab temperature decreases linearly from 0 to -10◦C between 0-2 m depth and only remains constant at -10◦C below 2 m depth, implies that a certain amount of warming has already taken place before the onset of the melt season. Field measurements of firn temperature (e.g. Humphrey and others, 2012; Machguth and others, 2016; MacFerrin and others, 2023) show that this a realistic assumption to account for and average out yearly and shorter-term variations in ice slab temperature.

CONCLUSIONS

We designed a simple, physics-based quasi 2D-model to describe lateral meltwater flow and superimposed ice formation atop near-surface ice slabs. The model was used to simulate four melt summers in the southwest of the Greenland ice sheet, and provides the development of water table- and snowpack height throughout the melt season, as well as values for the total amount of total discharge and meltwater retention in the form of newly formed superimposed ice.

Our results show that the evolution of the water table height and the occurrence or absence of a visible runoff limit is very dependent on the evolution and intensity of individual melt seasons. In general, less melt at higher altitudes leads to the later occurrence or absence of meltwater at the surface, although even in relatively colder melt seasons the water table can appear at the snow surface in case of short, intense melt events.

Changes in ice slab gradient play a major role in the appearance of of the visible runoff limit. Modelling results imply localised areas of slush formation in areas where the ice slab slope is flatter, which corresponds to observations made in the field and on satellite imagery.

Lateral flow is a very efficient mechanism for meltwater runoff: in any model grid cell lateral outflow is more than 30x larger than the amount of meltwater generated in situ. Measurements of snow and firn hydraulic properties exist, yet given the wide range of values provided by field observations, in particular

559 the hydraulic conductivity remains a source of uncertainty in the model. The model currently does not
560 include any mechanism for efficient meltwater drainage at the surface once the visible runoff limit has
561 appeared, but for further research this should be the first major enhancement to be made.

562 Superimposed ice formation can account for up to 40% of meltwater retention, and especially in case
563 of intermittent melt pulses this can drastically delay the occurrence of visible meltwater at the surface.
564 Values of modelled total SI formed (0.02-0.13 m w.e. throughout part of the melt season) roughly match
565 observations of ice slab thickening at KAN_U (0.28-0.37 m w.e. accretion of ice slab thickness per year).
566 Simplifications in the model, for example regarding the assumption of a fully isothermal snowpack and the
567 lack of internal meltwater refreezing should be considered; a better representation of the energy balance
568 would further improve the model.

569 In summary, our study highlights the pivotal role of lateral flow as a mechanism driving surface meltwa-
570 ter runoff. However, despite the insights gained from our simplified model, direct comparison with field- or
571 remote sensing data remains challenging. The complex nature of the hydrological processes at play makes
572 validation of results nontrivial. Efforts to enhance and expand the 1D-model are required and ongoing,
573 but the results presented in this paper are a first step towards a more comprehensive understanding and
574 description of the hydrological system in the accumulation zone of the southwestern Greenland ice sheet.

575 ACKNOWLEDGEMENTS

576 This study is funded by the European Research Council (ERC) under the European Union's Horizon 2020
577 research and innovation programme (project acronym CASSANDRA, grant agreement No. 818994). We
578 sincerely thank Bettina Schaefli and Nander Wever for their input and advice while shaping the model
579 design and strategy.

580 AUTHOR CONTRIBUTIONS

581 HM and NC designed the the study with contributions from AT. NC programmed the model with contri-
582 butions from HM and input data provided by DvA. NC carried out the model simulations and prepared
583 the manuscript with contributions from HM, AT and DvA.

REFERENCES

Ahlstrøm AP, Petersen D, Langen PL, Citterio M and Box JE (2008) A new programme for monitoring the mass loss of the Greenland ice sheet (doi: 10.34194/geusb.v15.5045)

Ahlstrøm AP, Petersen D, Langen PL, Citterio M and Box JE (2017) Abrupt shift in the observed runoff from the southwestern Greenland ice sheet. *Science Advances*, **3**(12) (doi: 10.1126/sciadv.1701169)

Baird PD (1952) Part I: Method of Nourishment of the Barnes Ice Cap. *Journal of Glaciology*, **2**(11), 2–9 (doi: 10.3189/S0022143000025910)

Bamber JL, Westaway RM, Marzeion B and Wouters B (2018) The land ice contribution to sea level during the satellite era. *Environmental Research Letters*, **13**(6), 1–19, ISSN 1748-9326 (doi: 10.1088/1748-9326/aac2f0)

Bartelt P and Lehning M (2002) A physical SNOWPACK model for the Swiss avalanche warning. *Cold Regions Science and Technology*, **35**(3), 123–145 (doi: 10.1016/s0165-232x(02)00074-5)

Bear J (1972) *Dynamics of fluids in porous media*. Dover Publications, ISBN 978-0-486-65675-5

Benson CS (1962) Stratigraphic studies in the snow and firn of the Greenland ice sheet. Research Report 70, U.S. Army Snow, Ice and Permafrost Research Establishment

Bøssing Christensen O, Drews M, Hesselbjerg Christensen J, Dethloff K, Ketelsen K, Hebestadt I and Rinke A (2007) The HIRHAM Regional Climate Model. Version 5 (beta)

Braithwaite RJ, Laternser M and Pfeffer WT (1994) Variations of near-surface firn density in the lower accumulation area of the Greenland ice sheet, Pâkitsoq, West Greenland. *Journal of Glaciology*, **40**(136), 477–485 (doi: 10.3189/s002214300001234x)

Brun E (1989) Investigation on wet-snow metamorphism in respect of liquid-water content. *Annals of Glaciology*, **13**, 22–26 (doi: 10.3189/S0260305500007576)

Calonne N, Geindreau C, Flin F, Morin S, Lesaffre B, du Roscoat SR and Charrier P (2012) 3-D image-based numerical computations of snow permeability: links to specific surface area, density, and microstructural anisotropy. *The Cryosphere*, **6**(5), 939–951 (doi: 10.5194/tc-6-939-2012)

Carman PC (1937) Fluid flow through granular beds. *Chemical Engineering Research and Design*, **75**, S32–S48 (doi: 10.1016/s0263-8762(97)80003-2)

Clerx N, Machguth H, Tedstone A, Jullien N, Wever N, Weingartner R and Roessler O (2022) In situ measurements of meltwater flow through snow and firn in the accumulation zone of the SW Greenland Ice Sheet. *The Cryosphere*, **16**(10), 4379–4401 (doi: 10.5194/tc-16-4379-2022)

Cogley J, Hock R, Rasmussen L, Arendt A, Bauder A, Braithwaite R, Jansson P, Kaser G, Möller M, Nicholson L and Zemp M (2011) Glossary of glacier mass balance and related terms. Technical Report 2, IACS, UNESCO-IHP, Paris

Coléou C and Lesaffre B (1998) Irreducible water saturation in snow: experimental results in a cold laboratory. *Annals of Glaciology*, **26**, 64–68 (doi: 10.3189/1998aog26-1-64-68)

Cox C, Humphrey N and Harper J (2015) Quantifying meltwater refreezing along a transect of sites on the Greenland icesheet. *The Cryosphere*, **9**, 691–701 (doi: 10.5194/tc-9-691-2015)

Culberg R, Schroeder DM and Chu W (2021) Extreme melt season ice layers reduce firn permeability across Greenland. *Nature Communications*, **12**(1) (doi: 10.1038/s41467-021-22656-5)

Culberg R, Chu W and Schroeder DM (2022) Shallow fracture buffers high elevation runoff in northwest Greenland. *Geophysical Research Letters*, **49**(23) (doi: 10.1029/2022gl101151)

Denoth A (1982) The pendular-funicular liquid transition and snow metamorphism. *Journal of Glaciology*, **28**(99), 357–364 (doi: 10.3189/s0022143000011692)

Enderlin EM, Howat IM, Jeong S, Noh MJ, van Angelen JH and van den Broeke MR (2014) An improved mass budget for the Greenland ice sheet. *Geophysical Research Letters*, **41**(3), 866–872 (doi: 10.1002/2013GL059010)

Fausto RS, van As D, Mankoff KD, Vandecrux B, Citterio M, Ahlstrøm AP, Andersen SB, Colgan W, Karlsson NB, Kjeldsen KK, Korsgaard NJ, Larsen SH, Nielsen S, Pedersen AØ, Shields CL, Solgaard AM and Box JE (2021) Programme for monitoring of the Greenland ice sheet (PROMICE) automatic weather station data. *Earth System Science Data*, **13**(8), 3819–3845 (doi: 10.5194/essd-13-3819-2021)

Fettweis X, Box JE, Agosta C, Amory C, Kittel C, Lang C, van As D, Machguth H and Gallée H (2017) Reconstructions of the 1900–2015 Greenland ice sheet surface mass balance using the regional climate MAR model. *The Cryosphere*, **11**(2), 1015–1033 (doi: 10.5194/tc-11-1015-2017)

Fountain AG and Walder JS (1998) Water flow through temperate glaciers. *Reviews of Geophysics*, **36**(3), 299–328 (doi: 10.1029/97rg03579)

Hanna E, Huybrechts P, Steffen K, Cappelen J, Huff R, Shuman C, Irvine-Fynn T, Wise S and Griffiths M (2008) Increased runoff from melt from the Greenland ice sheet: A response to global warming. *Journal of Climate*, **21**(2), 331–341 (doi: https://doi.org/10.1175/2007JCLI1964.1)

Harbaugh AW, Banta ER, Hill MC and McDonald MG (2000) Modflow-2000, the U.S. Geological Survey Modular ground-water model - user guide to modularization concepts and the ground-water flow process. Technical report, U.S. Geological Survey

643 Holmes CW (1955) Morphology and hydrology of the Mint Julep area, southwest Greenland. In *Project Mint Julep*
644 *Investigation of Smooth Ice Areas of the Greenland Ice Cap, 1953; Part II Special Scientific Reports*, Arctic, Desert,
645 Tropic Information Center; Research Studies Institute; Air University

646 How P, Abermann J, Ahlstrøm A, Andersen S, Box JE, Citterio M, Colgan W, Fausto R, Karlsson N, Jakobsen J, Lan-
647 gley K, Larsen S, Mankoff K, Pedersen A, Rutishauser A, Shield C, Solgaard A, Van As D, Vandecrux B and Wright
648 P (2022) PROMICE and GC-Net automated weather station data in Greenland (doi: 10.22008/FK2/IW73UU)

649 Humphrey NF, Harper JT and Pfeffer WT (2012) Thermal tracking of meltwater retention in greenland's accumu-
650 lation area. *Journal of Geophysical Research: Earth Surface*, **117**(F1), F01010 (doi: 10.1029/2011jf002083)

651 Jullien N, Tedstone AJ, Machguth H, Karlsson NB and Helm V (2023) Greenland ice sheet ice slab expansion and
652 thickening. *Geophysical Research Letters*, **50**(10) (doi: 10.1029/2022gl100911)

653 Koerner RM (1970) Some Observations on Superimposition of Ice on the Devon Island Ice Cap, N.W.T. Canada.
654 *Geografiska Annaler*, **52**(1), 57–67 (doi: 10.1080/04353676.1970.11879808)

655 Kollet SJ and Maxwell RM (2006) Integrated surface–groundwater flow modeling: A free-surface overland flow
656 boundary condition in a parallel groundwater flow model. *Advances in Water Resources*, **29**(7), 945–958 (doi:
657 10.1016/j.advwatres.2005.08.006)

658 Kozeny J (1927) Über kapillaire Leitung des Wassers im Boden. *Sitzungsberichte der Akademie der Wissenschaften*
659 *mathematisch-naturwissenschaftliche Klasse*, **136**, 271–306

660 Kuipers Munneke P, Ligtenberg SRM, van den Broeke MR, van Angelen JH and Forster RR (2014) Explaining the
661 presence of perennial liquid water bodies in the firn of the Greenland ice sheet. *Geophysical Research Letters*,
662 **41**(2), 476–483 (doi: 10.1002/2013gl058389)

663 Kuipers Munneke P, Ligtenberg SRM, Noël BPY, Howat IM, Box JE, Mosley-Thompson E, McConnell JR, Steffen
664 K, Harper JT, Das SB and van den Broeke MR (2015) Elevation change of the Greenland ice sheet due to surface
665 mass balance and firn processes, 1960–2014. *The Cryosphere*, **9**, 2009–2025

666 Kumar R, Samaniego L and Attinger S (2013) Implications of distributed hydrologic model parameterization on water
667 fluxes at multiple scales and locations. *Water Resources Research*, **49**(1), 360–379 (doi: 10.1029/2012wr012195)

668 Langen PL, Fausto RS, Vandecrux B, Mottram RH and Box JE (2017) Liquid water flow and retention on the
669 Greenland ice sheet in the regional climate model HIRHAM5: Local and large-scale impacts. *Frontiers in Earth*
670 *Science*, **4**, 110 (doi: 10.3389/feart.2016.00110)

671 Lehning M, Bartelt P, Brown B, Fierz C and Satyawali P (2002) A physical SNOWPACK model for the Swiss
672 avalanche warning: Part II: Snow microstructures. *Cold Regions Science and Technology*, **35**(3), 147–167 (doi:
673 10.1016/s0165-232x(02)00073-3)

674 Lemmelä R (1973) Measurements of evaporation-condensation and melting from a snowcover. In *The Role of Snow*
675 *and Ice in Hydrology*

676 Ligtenberg SRM, Helsen MM and van den Broeke MR (2011) An improved semi-empirical model for the densification
677 of Antarctic firn. *The Cryosphere*, **5**, 809–819 (doi: 10.5194/tc-5-809-2011)

678 MacFerrin M, Machguth H, van As D, Charalampidis C, Stevens CM, Heilig A, Vandecrux B, Langen PL, Mottram R,
679 Fettweis X, van den Broeke MR, Pfeffer WT, Moussavi MS and Abdalati W (2019) Rapid expansion of Greenland's
680 low-permeability ice slabs. *Nature*, **573**(7774), 403–407 (doi: 10.1038/s41586-019-1550-3)

681 MacFerrin MJ, Stevens CM, Vandecrux B, Waddington ED and Abdalati W (2023) The Greenland Firn Compaction
682 Verification and Reconnaissance (FirnCover) dataset, 2013–2019. *Earth System Science Data*, **14**(2), 955–971 (doi:
683 10.5194/essd-14-955-2022)

684 Machguth H, MacFerrin M, van As D, Box JE, Charalampidis C, Colgan W, Fausto RS, Meijer HA, Mosley-Thompson
685 E and van de Wal RS (2016) Greenland meltwater storage in firn limited by near-surface ice formation. *Nature*
686 *Climate Change*, **6**, 390–393 (doi: 10.1038/nclimate2899)

687 Machguth H, Tedstone AJ and Mattea E (2022) Daily variations in Western Greenland slush limits, 2000–2021.
688 *Journal of Glaciology*, **69**(273), 191–203 (doi: 10.1017/jog.2022.65)

689 Magnusson J, Wever N, Essery R, Helbig N, Winstral A and Jonas T (2015) Evaluating snow models with vary-
690 ing process representations for hydrological applications. *Water Resources Research*, **51**(4), 2707–2723 (doi:
691 10.1002/2014wr016498)

692 Marshall H, Conway H and Rasmussen L (1999) Snow densification during rain. *Cold Regions Science and Technology*,
693 **30**(1-3), 35–41 (doi: 10.1016/s0165-232x(99)00011-7)

694 Maxwell RM and Miller NL (2005) Development of a coupled land surface and groundwater model. *Journal of*
695 *Hydrometeorology*, **6**(3), 233–247 (doi: 10.1175/jhm422.1)

696 McDonald M and Harbaugh A (1988) A modular three-dimensional finite-difference ground-water flow model. resre-
697 port 83-875, U.S. Geological Survey

698 McGrath D, Colgan W, Bayou N, Muto A and Steffen K (2013) Recent warming at Summit, Greenland: Global
699 context and implications. *Geophysical Research Letters*, **40**(10), 2091–2096 (doi: 10.1002/grl.50456)

Meyer CR and Hewitt IJ (2017) A continuum model for meltwater flow through compacting snow. *The Cryosphere*, **11**, 2799–2813 (doi: 10.5194/tc-11-2799-2017)

Mikhalenko VN (1989) Osobennosti massoobmena lednikov ploskikh vershin vnutrennogo Tjan'-Shanja (Properties of mass exchange of plateau glaciers in the inner Tjan-Shan)). *Materials of glaciological studies*, **65**, 86–92

Miller O, Voss CI, Solomon DK, Miège C, Forster R, Schmerr N and Montgomery L (2022) Hydrologic modeling of a perennial firn aquifer in southeast Greenland. *Journal of Glaciology*, 1–16 (doi: 10.1017/jog.2022.88)

Miller OL, Solomon DK, Miège C, Koenig LS, Forster RR, Montgomery LN, Schmerr N, Ligtenberg SRM, Legchenko A and Brucker L (2017) Hydraulic conductivity of a firn aquifer in southeast Greenland. *Frontiers in Earth Science*, **5**(38) (doi: 10.3389/feart.2017.00038)

Mouginot J, Rignot E, Bjørk AA, van den Broeke M, Millan R, Morlighem M, Noël B, Scheuchl B and Wood M (2019) Forty-six years of Greenland ice sheet mass balance from 1972 to 2018. *Proceedings of the National Academy of Sciences*, **116**(19), 9239–9244 (doi: 10.1073/pnas.1904242116)

Müller F (1962) Zonation in the accumulation area of the glaciers of Axel Heiberg Island, N.W.T., Canada. *Journal of Glaciology*, **4**(33), 302–311 (doi: 10.3189/s0022143000027623)

Nghiem SV, Hall DK, Mote TL, Tedesco M, Albert MR, Keegan K, Shuman CA, DiGirolamo NE and Neumann G (2012) The extreme melt across the Greenland ice sheet in 2012. *Geophysical Research Letters*, **39**(20), L20502 (doi: 10.1029/2012gl053611)

Nienow PW, Sole AJ, Slater DA and Cowton TR (2017) Recent advances in our understanding of the role of meltwater in the Greenland ice sheet system. *Current Climate Change Reports*, **3**(4), 330–344 (doi: 10.1007/s40641-017-0083-9)

Noël B, van de Berg WJ, van Wessem JM, van Meijgaard E, van As D, Lenaerts JTM, Lhermitte S, Kuipers Munneke P, Smeets CJPP, van Ulft LH, van de Wal RSW and van den Broeke MR (2018) Modelling the climate and surface mass balance of polar ice sheets using RACMO2 – part 1: Greenland (1958–2016). *The Cryosphere*, **12**(3), 811–831 (doi: 10.5194/tc-12-811-2018)

Noël B, van de Berg WJ, Lhermitte S and van den Broeke MR (2019) Rapid ablation zone expansion amplifies north Greenland mass loss. *Science Advances*, **5**(9), eaaw0123 (doi: 10.1126/sciadv.aaw0123)

Obleitner F and Lehning M (2004) Measurement and simulation of snow and superimposed ice at the Kongsvegen glacier, Svalbard (spitzbergen). *Journal of Geophysical Research: Atmospheres*, **109**(D4) (doi: 10.1029/2003jd003945)

729 Parry V, Nienow P, Mair D, Scott J, Hubbard B, Steffen K and Wingham D (2007) Investigations of meltwater
730 refreezing and density variations in the snowpack and firn within the percolation zone of the Greenland ice sheet.
731 *Annals of Glaciology*, **46**, 61–68 (doi: 10.3189/172756407782871332)

732 Pfeffer WT and Humphrey NF (1998) Formation of ice layers by infiltration and refreezing of meltwater. *Annals of*
733 *Glaciology*, **26**, 83–91 (doi: 10.3189/1998aog26-1-83-91)

734 Pfeffer WT, Meier MF and Illangasekare TH (1991) Retention of Greenland runoff by refreezing: Implications for
735 projected future sea level change. *Journal of Geophysical Research*, **96**(C12), 22117 (doi: 10.1029/91jc02502)

736 Porter C, Morin P, Howat I, Noh MJ, Bates B, Peterman K, Keesey S, Schlenk M, Gardiner J, Tomko K, Willis
737 M, Kelleher C, Cloutier M, Husby E, Foga S, Nakamura H, Platson M, Wethington M, Williamson C, Bauer G,
738 Enos J, Arnold G, Kramer W, Becker P, Doshi A, D'Souza C, Cummens P, Laurier F and Bojesen M (2018)
739 "ArcticDEM", V1 (doi: 10.7910/DVN/OHHUKH)

740 Reeh N (1991) Parameterization melt rate and surface temperature on the Greenland ice sheet. *Polarforschung*, **59**,
741 113–128

742 Rennermalm ÅK, Hock R, Covi F, Xiao J, Corti G, Kingslake J, Leidman SZ, Miège C, Macferrin M, Machguth
743 H, Osterberg E, Kameda T and McConnell J (2021) Shallow firn cores 1989–2019 in southwest Greenland's
744 percolation zone reveal decreasing density and ice layer thickness after 2012. *Journal of Glaciology*, 1–12 (doi:
745 10.1017/jog.2021.102)

746 Samaniego L, Kumar R and Attinger S (2010) Multiscale parameter regionalization of a grid-based hydrologic model
747 at the mesoscale. *Water Resources Research*, **46**(5) (doi: 10.1029/2008wr007327)

748 Shimizu H (1970) Air permeability of deposited snow. *Contributions from the Institute of Low Temperature Science*,
749 1–32

750 Shumskii P (1964) *Principles of structural glaciology*. Dover Publications, New York

751 Smeets PCJP, Munneke PK, van As D, van den Broeke MR, Boot W, Oerlemans H, Snellen H, Reijmer CH and
752 van de Wal RSW (2018) The K-transect in west Greenland: Automatic weather station data (1993–2016). *Arctic,*
753 *Antarctic, and Alpine Research*, **50**(1) (doi: 10.1080/15230430.2017.1420954)

754 Smith LC, Yang K, Pitcher LH, Overstreet BT, Chu VW, Rennermalm ÅK, Ryan JC, Cooper MG, Gleason CJ,
755 Tedesco M, Jeyaratnam J, van As D, van den Broeke MR, van de Berg WJ, Noël B, Langen PL, Cullather RI, Zhao
756 B, Willis MJ, Hubbard A, Box JE, Jenner BA and Behar AE (2017) Direct measurements of meltwater runoff on
757 the Greenland ice sheet surface. *Proceedings of the National Academy of Sciences*, **114**(50), E10622–E10631 (doi:
758 10.1073/pnas.1707743114)

Steger CR, Reijmer CH, van den Broeke MR, Wever N, Forster RR, Koenig LS, Munneke PK, Lehning M, Lhermitte S, Ligtenberg SRM, Miège C and Noël BPY (2017) Firn meltwater retention on the Greenland ice sheet: A model comparison. *Frontiers in Earth Science*, **5**, 1–16 (doi: 10.3389/feart.2017.00003)

Stevens IT, Irvine-Fynn TD, Porter PR, Cook JM, Edwards A, Smart M, Moorman BJ, Hodson AJ and Mitchell AC (2018) Near-surface hydraulic conductivity of northern hemisphere glaciers. *Hydrological Processes*, **32**(7), 850–865 (doi: 10.1002/hyp.11439)

Tedesco M and Fettweis X (2020) Unprecedented atmospheric conditions (1948–2019) drive the 2019 exceptional melting season over the Greenland ice sheet. *The Cryosphere*, **14**(4), 1209–1223 (doi: 10.5194/tc-14-1209-2020)

Tedstone A and Machguth H (2022) Increasing surface runoff from greenland's firn areas. *Nature Climate Change* (doi: 10.1038/s41558-022-01371-z)

the IMBIE Team (2019) Mass balance of the greenland ice sheet from 1992 to 2018. *Nature*, **579**(7798), 233–239 (doi: 10.1038/s41586-019-1855-2)

van As D (2011) Warming, glacier melt and surface energy budget from weather station observations in the Melville Bay region of northwest Greenland. *Journal of Glaciology*, **57**(202), 208–220 (doi: 10.3189/002214311796405898)

van As D, Hubbard AL, Hasholt B, Mikkelsen AB, van den Broeke MR and Fausto RS (2012) Large surface meltwater discharge from the Kangerlussuaq sector of the Greenland ice sheet during the record-warm year 2010 explained by detailed energy balance observations. *The Cryosphere*, **6**(1), 199–209 (doi: 10.5194/tc-6-199-2012)

van As D, Box JE and Fausto RS (2016) Challenges of quantifying meltwater retention in snow and firn: An expert elicitation. *Frontiers in Earth Science*, **4**(101) (doi: 10.3389/feart.2016.00101)

van As D, Mikkelsen AB, Nielsen MH, Box J, Liljedahl LC, Lindbäck K, Pitcher L and Hasholt B (2017) Hypsometric amplification and routing moderation of Greenland ice sheet meltwater release. *The Cryosphere*, **11**, 1371–1386 (doi: 10.5194/tc-11-1371-2017)

van de Wal R, Greuell W, van den Broeke M, Reijmer C and Oerlemans J (2005) Surface mass-balance observations and automatic weather station data along a transect near Kangerlussuaq, west Greenland. *Annals of Glaciology*, **42**, 311–316 (doi: 10.3189/172756405781812529)

van de Wal RSW, Boot W, Smeets CJPP, Snellen H, van den Broeke MR and Oerlemans J (2012) Twenty-one years of mass balance observations along the K-transect, west Greenland. *Earth System Science Data*, **4**(1), 31–35 (doi: 10.5194/essd-4-31-2012)

van den Broeke M, Enderlin E, Howat I, Kuipers Munneke P, Noël B, van de Berg WJ, van Meijgaard E and Wouters B (2016) On the recent contribution of the Greenland ice sheet to sea level change. *The Cryosphere*, **10**, 1933–1946 (doi: 10.5194/tc-10-1933-2016)

van den Broeke M, Box J, Fettweis X, Hanna E, Noël B, Tedesco M, van As D, van de Berg WJ and van Kampenhout L (2017) Greenland ice sheet surface mass loss: Recent developments in observation and modeling. *Current Climate Change Reports*, **3**(4), 345–356 (doi: 10.1007/s40641-017-0084-8)

Vandecrux B, Mottram R, Langen PL, Fausto RS, Olesen M, Stevens CM, Verjans V, Leeson A, Ligtenberg S, Munneke PK, Marchenko S, van Pelt W, Meyer CR, Simonsen SB, Heilig A, Samimi S, Marshall S, Machguth H, MacFerrin M, Niwano M, Miller O, Voss CI and Box JE (2020) The firn meltwater Retention Model Intercomparison Project (RetMIP): evaluation of nine firn models at four weather station sites on the Greenland ice sheet. *The Cryosphere*, **14**(11), 3785–3810 (doi: 10.5194/tc-14-3785-2020)

Xiao J, Rennermalm ÅK, Covi F, Hock R, Leidman SZ, Miège C, MacFerrin MJ and Samimi S (2022) Local-scale spatial variability in firn properties in southwest Greenland. *Frontiers in Earth Science*, **10** (doi: 10.3389/feart.2022.938246)

Zuo Z and Oerlemans J (1996) Modelling albedo and specific balance of the Greenland ice sheet: calculations for the Søndre Strømfjord transect. *Journal of Glaciology*, **42**(141), 305–317 (doi: 10.3189/s0022143000004160)